ORIGINAL PAPER

Ab initio studies on the decomposition kinetics of CF_3OCF_2O radical

Hari Ji Singh · Bhupesh Kumar Mishra

Abstract The present study deals with the decomposition of CF_3OCF_2O radical formed from a hydrofluoroether, CF_3OCHF_2 (HFE-125), in the atmosphere. The study is performed using ab initio quantum mechanical methods. Two plausible pathways of decomposition of the titled species have been considered, one involving C-O bond scission and the other occurring via F atom elimination. The geometries of the reactant, products and transition states involved in the decomposition pathways are optimized and characterized at DFT (B3LYP) level of theory using 6-311G(d,p) basis set. Single point energy calculations have been performed at G2M(CC,MP2) level of theory. Out of the two prominent decomposition channels considered, the C-O bond scission is found to be dominant involving a barrier height of 15.3 kcal mol^{-1} whereas the F-elimination path proceeds with a barrier of 26.1 kcal mol^{-1}. The thermal rate constants for the above two decomposition pathways are evaluated using canonical transition state theory (CTST) and these are found to be $1.78 \times 10^6 \, s^{-1}$ and $2.83 \times 10^{-7} \, s^{-1}$ for C-O bond scission and F-elimination respectively at 298 K and 1 atm pressure. Transition states are searched on the potential energy surfaces involved during the decomposition channels and each of the transition states is characterized. The existence of transition states on the corresponding potential energy surface is ascertained by performing intrinsic reaction coordinate (IRC) calculation.

Keywords Canonical Transition State Theory · Decomposition of HFE · HFE-125 · PES

H. J. Singh (✉) · B. K. Mishra
Department of Chemistry, DDU Gorakhpur University,
Gorakhpur 273009, India
e-mail: hari_singh81@hotmail.com

Introduction

Concern over the global environmental consequences of fully halogenated chlorofluorocarbons (CFCs) has created a need to determine the potential impact of other halogenated organic compounds on stratospheric ozone. The absence of H-atom in the CFCs does not allow them to be oxidized or photolyzed in the troposphere. Thus, such compounds are transported into the stratosphere and their decomposition can lead to chlorine catalyzed ozone depletion [1–4]. Because of the critical role played by CFCs in stratospheric ozone depletion the search for the replacement of CFCs is a continuing process. HCFCs and HFCs have been found to be suitable alternatives and have been widely used in industrial applications [5, 6]. However, the release of HCFCs contributes to global warming and changes the global climate since they possess significant absorbing potential for the infrared (IR) radiation reflected from the earth's surface and are thus called the "greenhouse gases" (GHGs) [7, 8]. HFCs that have been used as interim replacements to CFCs and HCFCs have physicochemical, environmental and toxicological properties similar to that of the latters. However, there are some environmental hazards and health risks in using HFCs [9, 10]. Studies performed with many of the HFCs and HCFCs have shown that these are not a viable solution to protect the ozone layer because they possess significant global warming potential [11, 12]. Recently, attention has been paid to hydrofluoroethers (HFEs) to use it as third generation replacements of CFCs. It may find a place in the industry to be used as cleaning agents of electronic equipments, heat transfer agents in refrigeration systems and as carrier fluids for lubricant deposition [13–15]. One of the principal advantages of using HFEs is its shorter atmospheric lifetimes in comparison to HFCs as determined by Cooper et al. [16] using

computational methods. The shorter lifetimes of these HFEs lead to lower global warming potentials (GWPs) [17]. The absence of chlorine atoms in HFEs would lead us to believe that such compounds would have little impact on stratospheric ozone and would thus possess a negligible ozone depleting potential (ODP) [18, 19]. On the other hand, the presence of C-F and C-O bonds in HFEs may enhance the absorption features in the atmospheric infrared region (800–1400 cm^{-1}) and could play a significant role as greenhouse gases [20]. Therefore, there is an urgent need to perform experimental and theoretical studies on the decomposition of HFEs in order to find its suitability as a replacement of HCFCs and HFCs. Several theoretical and experimental studies performed on CHF_2OCHF_2 (HFE-134), CF_3OCH_3 (HFE-143a), $CF_3CF_2OCH_3$ (HFE-245cb2) and $CF_3CF_2CF_2OCH_3$ (HFE-347mcc3) have shown that these HFEs possess favorable physical and chemical properties to be used as suitable replacement of CFCs, HCFCs and HFCs [21, 22]. Like most HFEs, a general mechanism of tropospheric degradation mechanism of HFE-125 may be shown as follows (Scheme 1):

The above scheme is based on the fact that the initial attack of photochemically produced OH radical on HFE-125 leads to the formation of haloalkyl radical $(CF_3OCF_2{}^{\bullet})$. The latter reacts with atmospheric O_2 to produce peroxy radicals $(CF_3OCF_2O_2{}^{\bullet})$ which further react with NO_2 and ultimately form haloalkoxy radical $(CF_3OCF_2O{}^{\bullet})$ via a short-lived intermediate, the peroxynitrate $(CF_3OCF_2O_2NO_2)$. On the other hand, haloalkoxy

radical may also be generated through another intermediate, the hydroperoxide $(CF_3OCF_2O_2H)$ formed by the reaction of $CF_3OCF_2O_2$ and HO_2 radicals. In formulating a general mechanism for the atmospheric oxidation of hydrofluoroethers, Good et al. [23] proposed the following two plausible pathways of decomposition for the haloalkoxy radical, (CF_3OCF_2O) produced from HFE-125 as shown below:

$$CF_3OCF_2O \quad \rightarrow \quad CF_3O + CF_2O \quad\quad (1)$$

$$\rightarrow \quad CF_3OC(O)F + F. \quad\quad (2)$$
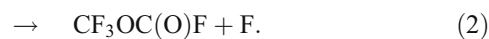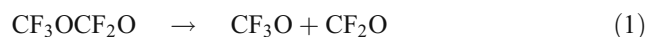
In addition to the above we also considered the decomposition to occur via

$$CF_3OCF_2O \quad \rightarrow \quad CF_3 + OCF_2O. \quad\quad (3)$$

The haloalkoxy radical (CF_3OCF_2O) studied during the course of the present investigation does not have any H-atom and therefore its reaction with O_2 is insignificant. The detailed calculation performed during the present investigation using DFT/B3LYP method show the endothermicity of reaction (3) to be more than 90 kcal mol^{-1} which makes it almost improbable. Thus, the most plausible fate of this radical in the atmosphere is its thermal decomposition as considered above by reactions (1) and (2). Recently, Murray et al. [24] analyzed the bond dissociation process in the case of simple diatomics and concluded that reaction force and force constant play a significant role in the atom separation processes. However, in the present study only

Scheme 1 Tropospheric degradation mechanism of HFE-125
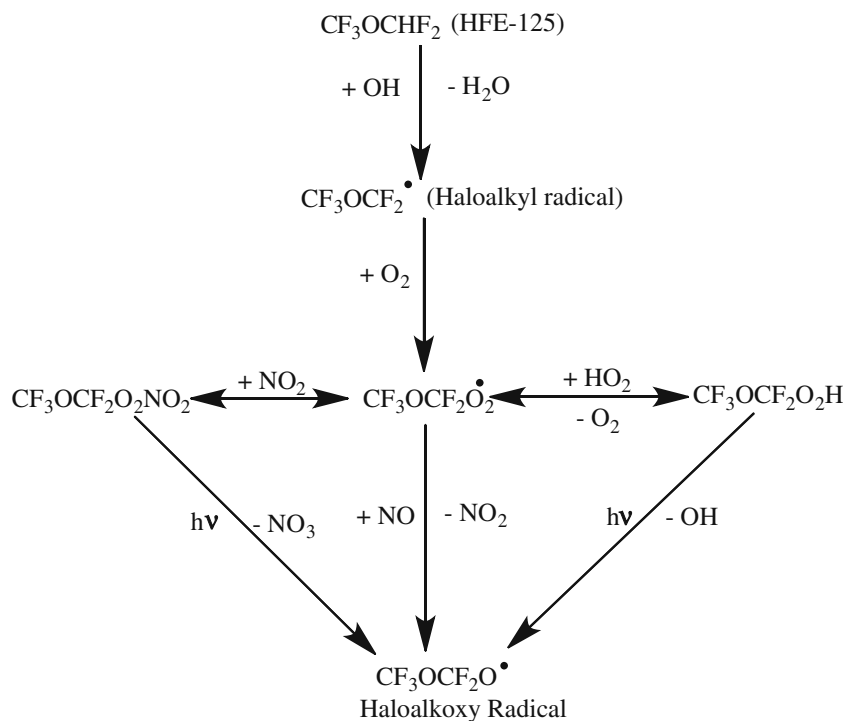
the thermal aspects of the bond dissociation processes have been considered and the energy barriers involved during the thermal decomposition have been calculated.

Due to the significant role played by haloalkoxy radicals formed from hydrofluoroethers in the destruction of a variety of organic compounds released into the atmosphere [25], there is a strong need for studying the fate of CF_3OCF_2O radical formed from HFE-125. There is no experimental data available in the literature to compare the theoretical results obtained by Good et al. [23] for the paths following the decomposition of hydrofluoroether (HFE-125) at DFT(B3LYP) level. In order to check the accuracy of the calculated values at DFT(B3LYP), there is a desirable need to perform high level ab initio quantum mechanical calculations. In the present investigation we performed a computational study using Möller-Plesset perturbation and coupled–cluster methods to determine the energetics involved in the decomposition pathways of CF_3OCF_2O radical involving C-O bond scission and F-elimination as given by reactions (1) and (2). G2M(CC, MP2) compound method is also used to calculate the

energy values of the species involved in the decomposition channels of the titled species. Rate constants for the above two channels considered are calculated by utilizing canonical transition state theory (CTST). Attempts have been made to search for transition states on the corresponding potential energy surfaces and energy barriers are calculated. Existence of transition states is ascertained by making intrinsic reaction coordinate (IRC) calculation.

Computational methods

Ab initio quantum mechanical calculations [26] were performed with the Gaussian 03 package [27]. Geometry optimization of the reactant, products and transition states were made using density functional study (DFT) employing Becke's three-parameter hybrid functional (B3LYP) [28, 29] with 6-311G(d,p) basis set. In order to determine the nature of different stationary points on the potential energy surface, vibrational frequencies were determined using the same level of theory at which the optimization

Fig. 1 Optimized geometries of reactant, products and transition states involved in the decomposition pathways of CF_3OCF_2O radical obtained at B3LYP/6-311G (d,p) level
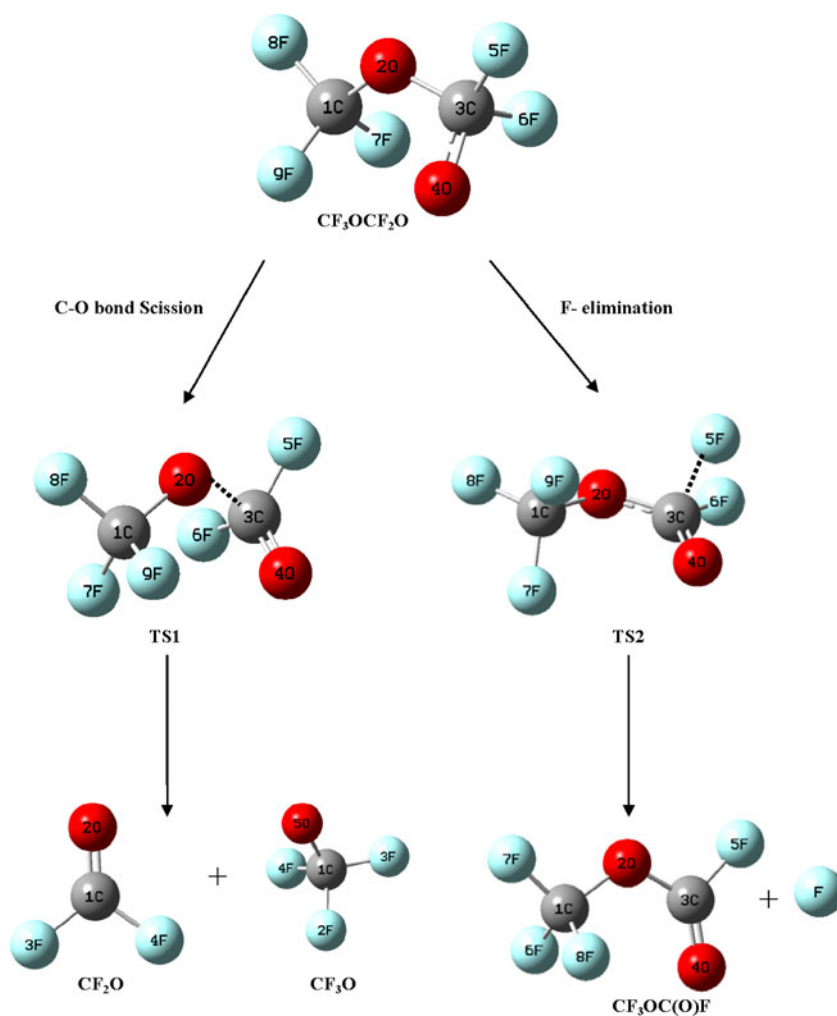
was made. All the stationary points have been identified to correspond to the minima with no imaginary frequency (NIMAG=0). Transition states are characterized by the presence of only one imaginary frequency (NIMAG=1). To ascertain that the identified transition states connect reactant and products smoothly, intrinsic reaction coordinate (IRC) calculations [30] were performed at B3LYP/6-311G(d,p) level. To obtain more reliable energies of various species along the PES, we used the G2M [31] method which

approaches high level results using a series of single point calculations for basis set size, correlation energy and systematic error corrections. Different versions of the G2M scheme have been suggested [31] however, Mebel et al. [32] found that G2M(CC,MP2) method yielded a considerably accurate value of energy for the systems containing six to seven heavy atoms. Thus, G2M(CC,MP2) method has been chosen for detailed calculation during the present study. The scheme is discussed here in brief. It uses

Table 1 Structural parameters of reactant, products and transition states involved in CF_3OCF_2O decomposition at B3LYP/6-311G(d,p) level of theory

	CF_3OCF_2O	TS1	TS2	CF_3O	CF_2O	$CF_3OC(O)F$
Bond length (Å)						
R (C1-O2)	1.387	1.372	1.401	–	1.170	1.391
R (C1-F2)	–	–	–	1.336	–	–
R (C1-F3)	–	–	–	1.336	1.321	–
R (C1-F4)	–	–	–	1.340	1.321	–
R (C1-F6)	–	–	–	–	–	1.329
R (C1-F7)	1.331	1.335	1.329	–	–	1.324
R (C1-F8)	1.325	1.338	1.322	–	–	1.329
R (C1-F9)	1.332	1.330	1.322	–	–	–
R (O2-C3)	1.399	1.784	1.340	–	–	1.357
R (C3-O4)	1.341	1.229	1.222	–	–	1.176
R (C3-F5)	1.338	1.315	1.885	–	–	1.324
R (C3-F6)	1.345	1.317	1.310	–	–	–
R (C1-O4)	–	–	–	–	–	–
R (C1-O5)	–	–	–	1.350	–	–
Bond angle (deg)						
A (O2-C1-F3)	–	–	–	–	126.196	–
A (O2-C1-F4)	–	–	–	–	126.196	–
A (O2-C1-F6)	–	–	–	–	–	111.450
A (O2-C1-F7)	112.509	113.103	110.695	–	–	105.954
A (O2-C1-F8)	105.759	105.218	105.427	–	–	111.453
A (O2-C1-F9)	111.449	111.954	111.823	–	–	–
A (F6-C1-F7)	–	–	–	–	–	109.351
A (F6-C1-F8)	–	–	–	–	–	109.205
A (F7-C1-F8)	109.411	108.922	109.502	–	–	109.350
A (F7-C1-F9)	108.558	108.387	109.509	–	–	–
A (F8-C1-F9)	109.074	109.134	109.798	–	–	–
A (C1-O2-C3)	121.639	121.624	119.291	–	–	118.218
A (O2-C3-O4)	107.664	92.508	126.905	–	–	129.029
A (O2-C3-F5)	105.101	98.383	104.942	–	–	105.839
A (O2-C3-F6)	112.560	104.730	107.565	–	–	–
A (O4-C3-F5)	113.834	122.593	82.331	–	–	125.130
A (O4-C3-F6)	110.550	122.438	123.200	–	–	–
A (F5-C3-F6)	107.103	108.756	99.669	–	–	–
A (F2-C1-F3)	–	–	–	107.538	–	–
A (F2-C1-F4)	–	–	–	109.521	–	–
A (F2-C1-F5)	–	–	–	112.443	–	–
A (F3-C1-O4)	–	–	–	109.521	–	–
A (F3-C1-F4)	–	–	–	–	107.606	–

Table 2 Unscaled vibrational frequencies of reactant, products and transition states involved in CF_3OCF_2O decomposition calculated at B3LYP/6-311G(d,p) level of theory

Species	Vibrational frequencies (cm^{-1})
CF_3OCF_2O	19, 104, 177, 277, 321, 356, 455, 473, 555, 576, 619, 673, 714, 843, 946, 1063, 1153, 1180, 1226, 1246, 1295
TS1	543i, 49, 85, 139, 246, 292, 359, 439, 525, 578, 588, 610, 657, 672, 889, 939, 1157, 1202, 1222, 1271, 1567
TS2	375i, 54, 95, 169, 203, 311,376, 410, 429, 550, 578, 632, 663, 737, 879, 1026, 1136, 1252, 1281, 1315, 1643
CF$_3$OC(O)F	74, 106, 179, 379, 403, 431, 553, 611, 671, 739, 774, 1051, 884, 1024, 1157, 1244, 1250, 1291, 1952
CF_3O	266, 403, 571, 590, 612, 889, 1152, 1202, 1260
CF_2O	578, 618, 774, 962, 1227, 1992

B3LYP/6-311G(d,p) optimized geometries and ZPE corrections and substitute the QCISD(T)/6-311G(d,p) calculation of the original G2 scheme [33] by the restricted open shell coupled cluster calculation [CCSD(T)/6-311G(d,p)] [34]. The total energy in G2M(CC,MP2) is calculated as:

$$E[G2M(CC, MP2)] = E_{base} + \Delta E(3df, 2p) + \Delta E(CC) + HLC + ZPE$$

where,

$$E_{base} = E[MP4/6 - 311G(d, p)],$$

$$\Delta E(3df, 2p) = E[MP2/6 - 311 + G(3df, 2p)]$$
$$- E[MP2/6 - 311G(d, p)], \text{ and}$$

$$\Delta E(CC) = E[CCSD(T)/6 - 311G(d, p)]$$
$$- E[MP4/6 - 311G(d, p)].$$

HLC (High Level Correction) $= -0.00525n_\alpha - 0.00019n_\beta$ (n_α and n_β are the number of α and β valence electrons with $n_\alpha \geq n_\beta$), and ZPE is zero-point energy obtained from vibrational frequency calculation performed at B3LYP/6-311G(d,p) level.

Results and discussion

Optimized geometries of reactants, products and transition states made at B3LYP /6-311G(d,p) level of theory are shown in Fig. 1 and their geometrical parameters are recorded in Table 1. Transition states are searched on the potential energy surface of reactions (1) and (2) and characterized as TS1 and TS2 respectively. Their optimized geometries are also shown in Fig. 1 and structural parameters are recorded in Table 1. Data recorded in Table 1 followed by visualization of the optimized structures using GaussView [35] reveal that in TS1 the elongation of the C—O bond occurs from 1.399 to 1.784Å resulting in an increase in the bond length of about 27%.

Similarly the results obtained for the optimized structure of TS2 reveal that C—F bond increases from 1.338Å to 1.885 Å (approx. 40%). Results obtained during frequency calculations performed at B3LYP/6-311G(d,p) level for species of reactions (1) and (2) and the corresponding transition states are recorded in Table 2. These results show that the reactants and products have stable minima on their potential energy surface characterized by the occurrence of only real positive vibrational frequencies. Transition states TS1 and TS2 are characterized by the occurrence of only one imaginary frequency obtained at 543 and 375 cm^{-1} respectively as recorded in Table 2. Visualization of the vibration corresponding to the calculated imaginary frequency using GaussView [35] shows a well defined transition state connecting reactants and products during transition. The existence of transition state on the potential energy surface is further ascertained by IRC calculation performed at the same level of theory. The minimum energy path is obtained by IRC calculation using Gonzalez—Schlegal steepest descent path [30] in the mass-weighted Cartesian coordinates with a step-size of 0.05 ($amu^{1/2}$-bohr) for each channel of decomposition. The IRC plots for
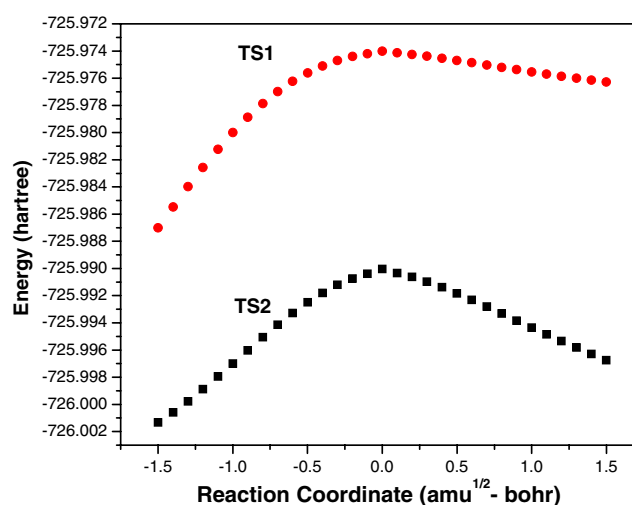
Fig. 2 IRC plots performed for transition states TS1 and TS2 obtained during thermal decomposition of CF_3OCF_2O

Table 3 Zero-point energy corrected total energies for species involved in CF_3OCF_2O decomposition. Geometries are optimized at B3LYP/6-311G(d,p) level. (unit: hartree)

Level	CF_3OCF_2O	TS1	TS2	$CF_3 + CF_2O$	$CF_3OC(O)F+F$
B3LYP/6-311++G(2d,2p)	−726.011157	−725.996742	−725.981780	−726.016588	−725.983153
MP2/6-311G(d,p)	−724.407948	−724.376095	−724.363203	−724.411435	−724.390130
MP2/6-311+G(3df,2p)	−724.839280	−724.807261	−724.791717	−724.837230	−724.812735
MP4/6-311G(d,p)	−724.478221	−724.450530	−724.436099	−724.480826	−724.459339
CCSD(T)/6-311G(d,p)	−724.468844	−724.444484	−724.429612	−724.469189	−724.446657
G2M(CC,MP2)	−725.065469	−725.040937	−725.023734	−725.061157	−725.062091

TS1 and TS2 are shown in Fig. 2 that clearly shows a smooth transition from reactants to products on the potential energy surface.

Single point energy calculations of various species involved in reactions (1) and (2) performed at MP2, MP4, CCSD(T) and DFT level of theories at B3LYP/6-311G(d,p) optimized geometries are recorded in Table 3. Zero point energy is determined at B3LYP/6-311G(d,p) and corrected with a scale factor of 0.96 [36]. Zero-point corrected total energies using standard and extended basis sets for various species under consideration are recorded in Table 3. Calculated energy values using G2M(CC,MP2) basis set additivity method is also recorded in Table 3. The associated energy barrier corresponding to reactions (1) and (2) determined from the data of Table 3 and recorded in Table 4 show that the energy barrier for C-O bond scission in CF_3OCF_2O is in the range of 9–20 kcal mol^{-1} depending upon the level of theory used during the calculation whereas it is in the range of 18–30 kcal mol^{-1} for F-elimination. The modified G2M(CC,MP2) method yields energy barriers as 15.3 and 26.1 kcal mol^{-1} for C-O bond scission and F-elimination respectively. The corresponding energy barriers calculated at B3LYP is found to be 9.0 and 18.4 kcal mol^{-1} as recorded in Table 4. The energy barriers for reactions (1) and (2) calculated during the present investigation at B3LYP/6-311++G(2d,2p) level are in close agreement with the values obtained by Good et al. [23] using B3LYP/6-311+G(2d,2p) method as 9.4 and

22.8 kcal mol^{-1}. It is observed that the energy barrier increases as we move to a higher level calculation. The calculated energy barriers as recorded in Table 4 for reactions (1) and (2) clearly show the dominance of C-O bond scission involved in the thermal decomposition of CF_3OCF_2O radical which is in accord with the conclusion made by Good et al. [23]. Using zero-point corrected total energy data as recorded in Table 3, an energy level diagram for reactions (1) and (2) is constructed. These energies are plotted with respect to the ground state energy of CF_3OCF_2O arbitrarily taken as zero. Results are shown in Fig. 3. It is evident from Fig. 3 that the C-O bond scission pathway is dominant as compared to F-elimination involved for thermal decomposition of CF_3OCF_2O. Calculations show that spin contamination is not important for the CF_3OCF_2O radical because $<S^2>$ is 0.76 at B3LYP/6-311G(d,p) before annihilation that are only slightly larger than the expected value of $S^2 = 0.75$ for doublets.

Rate constants

The rate constants of decomposition channels shown by reactions (1) and (2) of CF_3OCF_2O radical are calculated

Table 4 Calculated energy barriers in kcal mol^{-1}

Method	C-O bond scission	F-elimination
B3LYP/6-311++G(2d,2p)	9.0	18.4
MP2/6-311G(d,p)	19.9	28.0
MP2/6-311+G(3df,2p)	20.0	29.8
MP4/6-311G(d,p)	17.3	26.4
CCSD(T)/6-311G(d,p)	15.2	24.6
G2M(CC,MP2)	15.3	26.1
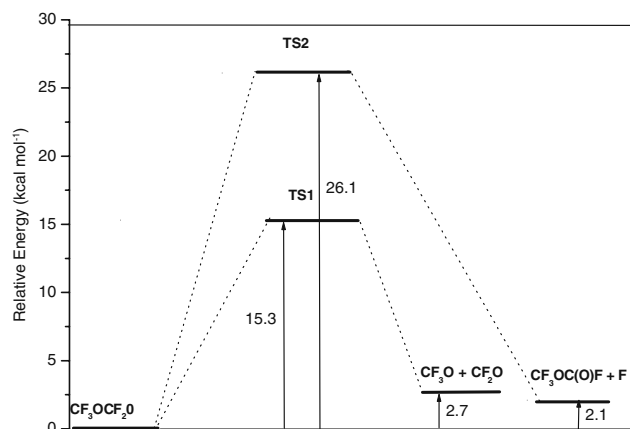
Fig. 3 Relative energy diagram in kcal mol^{-1} for the thermal decomposition of CF_3OCF_2O G2M(CC,MP2) levels

using canonical transition state theory (CTST) [37] using the following expression:

$$k = \Gamma(T) \frac{k_B T}{h} \frac{Q_{TS}^{\ddagger}}{Q_R} \exp\frac{-\Delta E}{RT} \qquad (4)$$

where $\Gamma(T)$ is the tunneling correction factor at temperature T. $Q_{TS}^{\ddagger}$ and Q_R are the total partition functions for the transition state and reactant respectively. ΔE, k_B and h are the barrier height, Boltzmann's and Planck's constants respectively. Calculation for the tunneling correction factor $\Gamma(T)$ is made using the expression of Wigner [38] as given by the expression:

$$\Gamma(T) = 1 + \frac{1}{24}\left(\frac{h\nu^{\#}}{k_B T}\right)^2 \qquad (5)$$

where $\nu^{\#}$ is the imaginary frequency at the saddle point. The tunneling correction factor $\Gamma(T)$ is found to be almost unity. The partition functions for the respective transition states and reactant are obtained from the vibrational frequency calculation performed at B3LYP/6-311G(d,p) level. The rate constant for C-O bond scission in CF_3OCF_2O decomposition is calculated to be $1.78 \times 10^6\,\mathrm{s}^{-1}$ at 298 K and 1 atm pressure which is of the same order of magnitude as that for the C-C bond scission determined by Somnitz and Zellner [39] in an anagolous hydrofluorocarbon (HFC-125).

The pre-exponential factor A for the unimolecular decomposition is evaluated from Eq. 6.

$$A = \frac{k_B T}{h} \frac{Q_{TS}^{\ddagger}}{Q_R} \qquad (6)$$

The terms used in Eq. 6 have their usual meaning as discussed above. Our modeling calculation yields the A-factor for C-O bond scission to be $0.46 \times 10^{13}\,\mathrm{s}^{-1}$ which is in good agreement with a value of $1.1 \times 10^{13}\,\mathrm{s}^{-1}$ calculated by Henon et al. [40] for β-C-O scission in other oxygenated alkoxy radicals. Similar calculations performed to determine the rate constant for F-elimination via reaction (2) involving TS2 as the transition state yielded a value of $2.83 \times 10^{-7}\,\mathrm{s}^{-1}$ at 298 K and 1 atm pressure with the associated A-factor of $3.68 \times 10^{12}\,\mathrm{s}^{-1}$.

Conclusions

The most important stationary points on the potential energy surface for the thermal decomposition of CF_3OCF_2O radical are investigated at G2M(CC,MP2)//B3LYP/6-311G(d,p) level of theory. Energetic calculation reveals that the most dominant decomposition pathway for CF_3OCF_2O is the C-O bond scission that occurs with a barrier height of 15.3 kcal mol^{-1} whereas the F-elimination process occurs with an energy barrier of 26.1 kcal mol^{-1}. The thermal rate constants evaluated using conventional transition state theory for reactions (1) and (2) are found to be $1.78 \times 10^6\,\mathrm{s}^{-1}$ and $2.83 \times 10^{-7}\,\mathrm{s}^{-1}$ respectively with the corresponding A-factor as 0.46×10^{13} and $3.68 \times 10^{12}\,\mathrm{s}^{-1}$ at 298 K and 1 atm pressure.

References

1. Solomon S (1990) Nature (London) 6291:347–354
2. Molina MJ, Rowland FS (1974) Nature 249:810–814
3. Rowland FS, Molina MJ (1994) Chem Eng News 8:72–76
4. Weubbles DJ (1983) J Geophys Res 88:1433–1443
5. Scientific Assessment of Stratospheric Ozone (1989) Vol 11; World Meteorological Organization, Global Ozone Research and Monitoring Project Report No. 20, Geneva
6. Wayne RP (2001) Chemistry of atmospheres. Clarendon press, Oxford
7. Dekant W (1996) Environ Health Perspect 104:75–83
8. Hayman G, Derwent RD (1997) Environ Sci Technol 31:327–336
9. Tsai WT, Chen HP, Hsien WY (2002) J Loss Prev Process Ind 15:65–75
10. Tsai WT (2005) Chemosphere 61:1539–1547
11. Pinnock S, Hurly M, Shine KP, Wallington TJ, Smyth TJ (1995) J Geophys Res 100:23227–23238
12. International Panel on Climate Change (IPCC) (1996) Climate change 1995: the science of climate change. Cambridge University Press, New York
13. Tsai WT (2005) J Hazard Mater 119:69–78
14. Sekiya A, Misaki S (2000) J Fluorine Chem 101:215–221
15. Bivens DB, Minor BH (1998) Int J Refrig 21:567–576
16. Cooper DL, Cunningham TP, Allan NL, McCulloch A (1992) Atmos Environ 26A:1331–1334
17. Blowers P, Tetrault KF, Morehead YT (2008) Theor Chem Acc 119:369–381
18. Ravishankara RA, Turnipseed AA, Jensen NR, Barone S, Mills M, Howark CJ, Solomon S (1994) Science 263:71–75
19. Granier C, Shine KP, Daniel JS, Hansen JE, Lal S, Stordal F (1999) Climate effects of ozone and halocarbon changes, in scientific Assessment of Ozone Depletion: 1998 Rep. 44, Global Ozone Research and Monitoring Project. World Meteorological Organization, Geneva
20. Good DA, Francisco JS (1998) J Phys Chem 102:1854–1864
21. Sekiya A, Misaki S (1996) Chemtech 26:44–48
22. Smith ND (1992) EPA-60/F-92-012. Springerfield
23. Good DA, Mike K, Randy S, Francisco JS (1999) J Phys Chem 103:9230–9240
24. Murray JS, Toro-Labbe A, Clark T, Politzer P (2009) J Mol Model 15:701–706
25. Atkinson R (1990) Atoms Environ 24A:1–41
26. Hehre WJ, Radom L, PvR S, Pople JA (1986) Ab initio molecular orbital theory. Wiley, New York
27. Frisch MJ, Trucks GW, Schlegel HB et al (2003) Gaussian 03, Rev C.02. Gaussian Inc, Pittsburgh
28. Becke AD (1993) J Chem Phys 98:5648–5652

29. Lee C, Yang W, Parr RG (1988) Phys Rev B 37:785–789
30. Gonzalez C, Schlegel HB (1990) J Chem Phys 94:5523–5527
31. Curtiss LA, Raghavachari K, Trucks GW, Pople JA (1991) J Chem Phys 94:7221–7230
32. Mebel AM, Morokuma K, Lin MC (1995) J Chem Phys 103:7414–7421
33. Curtiss LA, Redfern PC, Smith BJ, Radom L (1996) J Chem Phys 104:5148–5164
34. Purvis GD, Bartlett RJ (1982) J Chem Phys 76:1910–1918
35. Frisch A, Nielsen AB, Holder AJ (2000) GaussView reference. Gaussian Inc, Wallingford
36. Scott AP, Radom L (1996) J Phys Chem 100:16502–16513
37. Truhlar DG, Garrett BC, Klippenstein SJ (1996) J Phys Chem 100:12771–12800
38. Wigner EP (1932) Z Phys Chem B19:203–216
39. Somnitz H, Zellner R (2001) Phys Chem Chem Phys 3:2352–2364
40. Henon E, Bohr F, Sokolowski Gomez N, Caralp F (2003) Phys Chem Chem Phys 5:5431–5437